Received: 27 January 2024 | Revised: 8 June 2024 | Accepted: 24 June 2024

DOI: 10.1096/fj.202400213RR

RESEARCH ARTICLE

The FASEB Journal

Impaired myoblast differentiation and muscle IGF-1 receptor signaling pathway activation after N-glycosylation inhibition

Giosuè Annibalini[1] | **Laura Di Patria**[1] | **Giacomo Valli**[2] | **Matteo Bocconcelli**[1] | **Roberta Saltarelli**[1] | **Lorenzo Ferri**[3] | **Laura Barberi**[4] | **Fabiana Fanelli**[1] | **Amelia Morrone**[3,5] | **Rita Barone**[6,7] | **Renzo Guerrini**[3,5] | **Antonio Musarò**[4] | **Vilberto Stocchi**[8] | **Elena Barbieri**[1]

[1]Department of Biomolecular Sciences, University of Urbino Carlo Bo, Urbino, Italy

[2]Department of Clinical and Experimental Sciences, University of Brescia, Brescia, Italy

[3]Department of Neuroscience and Medical Genetics, Meyer Children's Hospital IRCCS, Florence, Italy

[4]DAHFMO-Unit of Histology and Medical Embryology, Laboratory Affiliated to Istituto Pasteur Italia, University of Rome La Sapienza, Rome, Italy

[5]Department of NEUROFARBA, University of Florence, Florence, Italy

[6]Child Neurology and Psychiatry Unit, Department of Clinical and Experimental Medicine, University of Catania, Catania, Italy

[7]Research Unit of Rare Diseases and Neurodevelopmental Disorders, Oasi Research Institute-IRCCS, Troina, Italy

[8]Department of Human Sciences for the Promotion of Quality of Life, University San Raffaele, Rome, Italy

Correspondence
Giosuè Annibalini, Department of Biomolecular Sciences, University of Urbino Carlo Bo, Via I Maggetti, 26/2, Urbino 61029, Italy.
Email: giosue.annibalini@uniurb.it

Funding information
Next Generation EU PRIN 2022, Grant/Award Number: 202255RLB4 and 2022LZARA3; University of Urbino Carlo Bo, Grant/Award Number: 446/2020; AFM-Telethon, Grant/Award Number: 23608; Fondazione Roma, Grant/Award Number: 2022/2025

Abstract

The role of N-glycosylation in the myogenic process remains poorly understood. Here, we evaluated the impact of N-glycosylation inhibition by Tunicamycin (TUN) or by *phosphomannomutase 2* (*PMM2*) gene knockdown, which encodes an enzyme essential for catalyzing an early step of the N-glycosylation pathway, on C2C12 myoblast differentiation. The effect of chronic treatment with TUN on tibialis anterior (TA) and extensor digitorum longus (EDL) muscles of WT and MLC/mIgf-1 transgenic mice, which overexpress muscle *Igf-1Ea* mRNA isoform, was also investigated. TUN-treated and *PMM2* knockdown C2C12 cells showed reduced ConA, PHA-L, and AAL lectin binding and increased ER-stress-related

Abbreviations: AAL, Aleuria Aurantia (AAL); AKT, Serine/threonine protein kinase B; CCND1, Cyclin D1; CDG, Congenital Disorders of Glycosylation; Chop, C/EBP homologous protein; Con A, Concanavalin A; CRISPR/Cas9, Clustered regularly interspaced short palindromicrepeats/CRISPR-associated protein 9; CTR, Control; DAPI, 2-(4-amidinophenyl)-1H-indole-6-carboxamidine; DMEM, Dulbecco's Modified Eagle Medium; EDL, Extensor digitorum longus muscle; FBS, Fetal bovine serum; GAPDH, Glyceraldehyde-3-PhosphateDehydrogenase; Glc-1,6-P_2, glucose1,6-bisphosphate; HEK293, Human embryonic kidney 293 cells; HRP, Horseradish peroxidase; Hspa5, Heat Shock Protein FamilyA (Hsp70) Member 5; IGF-1, Insulin-like growth factor-1; IGF1R, IGF-1 receptor; IR, Insulin Receptor; MF20, Myosin heavy chain; MRF, Myogenic regulatory factors; Mrf4, Myogenic Factor 6; Myf5, Myogenic Factor 5; MyoD, Myogenic differentiation 1; NADP+, oxidized nicotinamide adenine dinucleotide phosphate; NADPH, reduced nicotinamide adenine dinucleotidephosphate; OST, Oligosaccharyltransferase; PBS, Phosphate buffered saline; PCNA, Proliferating Cell NuclearAntigen; PHA-L, Phaseolus vulgaris leucoagglutinin; PI3K, Phosphatidylinositol 3 kinase; PMM2, Phosphomannomutase 2; SA-βgal, Senescence-associated beta-galactosidase; TA, Tibialis anterior muscle; TUN, Tunicamycin; WT, wild type; Xbp1, spliced X-box binding protein 1.

gene expression (*Chop* and *Hspa5* mRNAs and *s/uXbp1* ratio) compared to controls. Myogenic markers (*MyoD, myogenin*, and *Mrf4* mRNAs and MF20 protein) and myotube formation were reduced in both TUN-treated and *PMM2* knockdown C2C12 cells. Body and TA weight of WT and MLC/mIgf-1 mice were not modified by TUN treatment, while lectin binding slightly decreased in the TA muscle of WT (ConA and AAL) and MLC/mIgf-1 (ConA) mice. The ER-stress-related gene expression did not change in the TA muscle of WT and MLC/mIgf-1 mice after TUN treatment. TUN treatment decreased *myogenin* mRNA and increased *atrogen-1* mRNA, particularly in the TA muscle of WT mice. Finally, the IGF-1 production and IGF1R signaling pathways activation were reduced due to N-glycosylation inhibition in TA and EDL muscles. Decreased IGF1R expression was found in TUN-treated C2C12 myoblasts which was associated with lower IGF-1-induced IGF1R, AKT, and ERK1/2 phosphorylation compared to CTR cells. Chronic TUN-challenge models can help to elucidate the molecular mechanisms through which diseases associated with aberrant N-glycosylation, such as Congenital Disorders of Glycosylation (CDG), affect muscle and other tissue functions.

KEYWORDS

congenital disorders of glycosylation, glycosylation, IGF1R signaling pathway, muscle atrophy, myoblast differentiation, *PMM2*

1 | INTRODUCTION

Myogenesis is a complex and highly regulated process that requires myoblast proliferation, alignment of cells, and subsequent fusion into multinucleated myotubes.[1] Many steps of myogenesis can be recapitulated *in vitro* through myogenic cell lines such as mouse C2C12 and rat L6E9, which in the absence of mitogenic stimuli form multinucleated myotubes.[1] The myogenic process depends on a complex network of signal transduction pathways regulating the expression of myogenic regulatory factors (MRFs), a group of basic helix–loop–helix transcription factors that include MyoD, Myf5, myogenin, and Mrf4.[1,2] Besides the canonical MRF, other molecules such as insulin-like growth factor-1 (IGF-1) are directly involved in the myogenesis process.[3] The primary effects of IGF-1 are mediated by binding to the IGF-1 receptor (IGF1R), a ligand-activated receptor tyrosine kinase. IGF1R signal transduction occurs through the PI3K/AKT/mTOR and RAF/MEK/ERK pathways which promote muscle protein synthesis and inhibit muscle protein degradation.[4] Recent studies showed that both IGF-1 and IGF1R are synthetized as pre-protein precursors which are extensively processed to allow IGF-1 secretion and the formation of functional IGF1R, respectively.[5–9] In particular, IGF-1 is synthesized as a larger prohormone that is subsequently converted into mature IGF-1 by furin cleavage of its C-terminal extension named E-peptide. Due to alternative splicing of the *Igf-1* gene, three different E-peptides may be produced: Ea-, Eb-, and Ec-peptides (named according to human nomenclature). Ea-peptide contains two N-glycosylation sites in mice,[9,10] one of which is also conserved in humans (N92).[5] We demonstrated that N-glycosylation of the human IGF-1Ea prohormone is necessary for efficient IGF-1 secretion.[5] On the other hand, both the IGF-1Eb and IGF-1Ec prohormones lacked putative N-glycosylation sites, and their production appears to be largely unaffected by glycosylation.[5] Proper N-glycosylation is essential also for IGF1R translocation to the plasma membrane and for IGF-1-induced activation.[6–8,11] Thus, the IGF-1 signaling pathway seems to be particularly sensitive toward N-glycosylation.[12] Growing evidence highlights the role of protein glycosylation in myoblast fusion and differentiation.[13–17] Gundry R.L. et al. identified 128 glycosylated proteins in the C2C12 myoblast cell surface, including Insulin Receptor (IR) and IGF1R.[18] More recently, Blazev R. et al. demonstrated a dynamic change in proteomic, N-glycomic, and N-glycoproteomic during rat L6 myotube formation.[17] Interestingly, the abundance of lectins and enzymes involved in glycan biosynthesis and remodeling were modulated after the differentiation of myoblasts toward myotubes, suggesting that temporal- and site-specific glycosylation tuning is important for skeletal muscle cell development, differentiation, and function.[17] During myoblast differentiation, increased binding of lectins with different carbohydrate specificities[19,20] and regulation of N-glycan content of glycoproteins,[17] including several integrins and growth factor receptors, has been shown.

The effects of incorrect protein muscle glycosylation in humans are illustrated by dystroglycanopathies, a group of inherited genetic diseases caused by defective O-mannosylation of α-Dystroglycan.[21] However, the consequence of aberrant protein N-glycosylation in muscle homeostasis remains poorly understood. Early evidence showed that fusion of embryonic quail muscle cells is impaired by Tunicamycin (TUN), an antibiotic that inhibits the Dolichyl-Phosphate N-Acetylglucosaminephosphot ransferase 1 (DPAGT1) enzyme which catalyzes the first step of the N-glycosylation pathway.[22] More recently, Xia et al. demonstrated that administration of TUN increases ER-stress markers in the liver, decreases hepatic *Igf-1* mRNA expression and IGF-1 serum levels, and reduces body growth and body weight gain in C57BL/6J mice.[23] However, the impact of TUN on muscle tissues is still unknown.

A wide spectrum of neuromuscular syndromes ranging from muscle dystrophy to congenital myopathy/myasthenic syndrome has been associated with Congenital Disorders of Glycosylation (CDG) caused by N-glycosylation defects.[24] CDGs are inborn errors of metabolism following a Mendelian pattern of inheritance characterized by "substantial hypoglycosylation in one or more cell types".[25] Over 160 CDG types and more than 200 phenotypes have been characterized.[25] The most common type is PMM2-CDG, caused by pathogenetic variants in the *PMM2* gene encoding the enzyme phosphomannomutase 2 (PMM2) that converts mannose-6-phosphate into mannose-1-phosphate, the obligatory precursor for GDP-mannose production and hence N-linked glycosylation.[26] The global suppression of N-glycosylation in PMM2-CDG affects multiple systems leading to a variety of symptoms. Patients with PMM2-CDG exhibit prominent cerebellar ataxia due to progressive cerebellar atrophy in addition to other neuromuscular symptoms such as peripheral neuropathy which leads to causes functional disability and wheelchair dependence.[27,28] The rate and the severity of myopathy in PMM2-CDG have not been extensively explored.

In the present study, we evaluate the consequences of N-glycosylation inhibition on myoblast differentiation by TUN administration or *PMM2* knockdown in mouse C2C12 model cells. Moreover, 6-week-old wild-type (WT) and MLC/mIgf-1 transgenic FVB mice, which overexpress the *Igf-1Ea* isoform under the control of the myosin light chain (MLC) promoter,[29] were chronically challenged with a sub-phenotypic dose of TUN to mimic a mild CDG-like phenotype. Tibialis anterior (TA) and extensor digitorum longus (EDL) muscles were collected to evaluate the impact of N-glycosylation inhibition on lectin binding, ER-stress-related gene expression, and IGF-1 signaling pathway activation.

2 | MATERIALS AND METHODS

2.1 | Cell cultures

C2C12 mouse myoblasts (Sigma-Aldrich, Italy), CRISPR-CTR and CRISPR-PMM2 C2C12, and rat L6E9 myoblasts[30] were cultured in Dulbecco's Modified Eagle Medium (DMEM) supplemented with 10% heat-inactivated fetal bovine serum (FBS), 2 mM glutamine, penicillin (100 U/mL), and streptomycin (100 μg/mL), and maintained in a 5% CO_2 atmosphere at 37°C. To induce C2C12 myogenic differentiation, C2C12 myoblasts at 80%–90% confluence were transferred to a differentiation medium (DM) containing 2% horse serum, as previously described.[31] To activate myogenic differentiation of rat L6E9, myoblasts were switched to a DM containing DMEM plus 1% bovine serum albumin.[30] The C2C12 was maintained in the DM for 6 days, while L6E9 for 4 days. For TUN (cat. no. T7765; Sigma-Aldrich) treatment, C2C12 and L6E9 myoblasts were incubated with 0.01 μg/mL of TUN for 24 h and then for 6 days (C2C12) or 4 days (L6E9) in the DM. The medium was changed every 2 days along with fresh DMSO (control) or TUN treatment. Cells were harvested on day 1 (C2C12 and L6E9) and days 4 (L6E9) and 6 (C2C12) after the induction of the differentiation. C2C12 myoblasts concentration and viability were determined by LUNA-II™ Automated Cell Counter (Logos Biosystems, Twin Helix) with trypan blue staining. Cytotoxicity was calculated as follows: Cytotoxicity (%)=[(dead cell number/total cells)×100]. All cell lines were routinely screened for the absence of mycoplasm contamination by PCR using the Mycoplasm Detection kit (abm, cat. num G238, SIAL srl, Italy). All mutant cell lines are available from the authors upon request.

2.2 | WT and MLC/mIgf1 transgenic mice

Jackson Laboratories' FVB female mice were utilized as embryo donors for the generation of MLC/mIgf1 transgenic animals, as previously described.[29] Animals were kept in ventilated cages (4–5 per cage) in a room with constant temperature (22°C) and humidity (45%–55%), and with 12:12 h light/dark cycle. Each cage was equipped with wood shavings, bedding and a cardboard tube for enrichment and spontaneous physical activities. The mice had access to a constant supply of food (Teklad Global 18% Protein Rodent Diet; Envigo, Huntingdon, UK) and water. Every four months, sentinel mice were examined for any potential infection listed in the FELASA recommendations. Female WT and MLC/mIgf1 transgenic animals of 6 weeks of age were used for all the experiments. Animals

were randomly allocated to sham or TUN groups. The research project was conducted according to the animal welfare regulations and guidelines and approved by the Institutional Review Board of the animal facilities of the National Institute of Health—Italy.

2.3 | PMM2 knockdown by CRISPR/Cas9

For CRISPR/Cas9 silencing, 5.0×10^4 C2C12 cells/well were seeded in 12-well plates and transfected with 1 μg of the PMM2 Double-Nickase plasmid (cat. no. sc-424790-NIC; Santa Cruz Biotechnology, D.B.A. Italia) or the corresponding Double-Nickase Control plasmid (cat. no. sc-437281; Santa Cruz Biotechnology, D.B.A. Italia) using the TransIT-X2® Transfection Reagent (Mirus Bio, TEMA ricerca) for 48 h. Following the manufacturer's protocol, the selection was performed with puromycin (cat. no. P9620; Sigma-Aldrich), and clones were screened by qRT-PCR and PMM enzymatic activity assay. Three C2C12 myoblast clones with a marked reduction of *PMM2* mRNA expression and PMM enzymatic activity were selected for further analyses.

2.4 | PMM enzymatic activity assay

CRISPR-CTR and CRISPR-PMM2 C2C12 cells were washed twice in PBS, scraped, pelleted by centrifugation, and re-suspended in lysis buffer (20 mM Hepes, 25 mM KCl, 1 mM dithiothreitol, and 1× protease inhibitor mixture) and then briefly sonicated and incubated at 4°C for 15 min. Afterward, the cell lysates were centrifuged at 15 000 rpm for 10 min at 4°C to remove cellular debris. Protein concentration of each freshly prepared cell lysate was determined with Bradford Reagent (Sigma-Aldrich). PMM enzymatic activity was assayed as reported by Van Schaftingen and Jaeken[32] with slight modification. Briefly, PMM activity was measured at 32°C in Hepes 20 mM pH 7.5 containing $MgCl_2$ 5 mM, $NADP^+$ 0.25 mM, in the presence of 0.3 mM Mannose-1-P as the substrate, 1 μM Glc-1,6-P_2 as the activator, 2.8 U/mL glucose 6-phosphate dehydrogenase, 3.7 U/mL phosphoglucose isomerase, and 3.9 μg/mL phosphomannose isomerase. The reaction started by adding 50 μg/mL of cell lysates. The activity was followed spectrophotometrically for 60 min at 340 nm, recording the reduction of $NADP^+$ to NADPH. One unit is the amount of enzyme that catalyzes the conversion of 1 μmol of substrate per min under this condition.

2.5 | Immunofluorescence

C2C12 and L6E9 cell cultures were washed with phosphate-buffered saline (PBS) (8 g/L NaCl, 1.15 g/L Na_2HPO_4, 0.2 g/L KH_2PO_4, 0.2 g/L KCl), fixed for 15 min at room temperature with 4% formaldehyde/PBS and permeabilized in 0.5% Triton X-100/PBS for 4 min. A mouse monoclonal antibody against Myosin heavy chain (MF20 at the 1:2 dilution; obtained from DSHB) was incubated at 37°C for 1 h followed by incubation at 37°C for a 30-min with 1:100 fluorescein-conjugated goat anti-mouse IgG (Biolegend, San Diego, CA, USA). An antibody against total IGF1R β (1:1000; cat. n. 3027 Cell Signaling Technology) was incubated at room temperature for 1 h followed by incubation at room temperature for 1 h with 1:200 Rhodamine Red™-X (RRX) AffiniPure™ Goat Anti-Rabbit IgG (H+L) (Jackson ImmunoResearch Europe Ltd.). Cells were stained with DAPI (2-(4-amidinophenyl)-1H-indole-6-carboxamidine) for nuclear visualization and mounted in Mowiol 4-88 (Sigma-Aldrich) slides. Images were acquired using the TOUPCAM™ E31SPM05000KPA digital camera connected to a Leica microscope DMLB and the ToupView software. Fusion index was determined by counting the number of nuclei in differentiated myotubes using ImageJ software and expressed as a percentage of the total number of nuclei.

2.6 | RNA extraction, cDNA synthesis, and qRT-PCR

Total RNA was extracted and purified using the Omega Bio-Tek E.Z.N.A.™ Total RNA kit (VWR International) according to the manufacturer's instructions. The amount of RNA was assessed with SpectraMax® QuickDrop™ Micro-Volume Spectrophotometer (Molecular Devices, CaRli biotec), and the complementary DNA was synthesized from 500 ng of total RNA using Takara PrimeScript™RT Master Mix (Takara Bio Inc., Diatech Lab Line Srl). Subsequently, quantitative RT-PCR (qRT-PCR) was performed with 2 μL of cDNA and 300 nM of each primer in an Applied Biosystems StepOnePlus™ Real-Time PCR System using PowerUp SYBR Green Master Mix (Applied Biosystems). The qRT-PCR conditions were 50°C for 2 min, 95°C for 2 min followed by 40 cycles of two steps at 95°C for 15 s, and 60°C for 60 s. The relative mRNA expression of target genes was normalized to *gapdh* internal control. The genes of interest and the sequence of the specific primer used in qRT-PCR quantification are listed in Table S1.

2.7 | Immunoblotting and lectin blotting

Cells were lysed adding 40–60 μL of lysis buffer containing: 20 mM HEPES (pH 7.9), 25% v/v glycerol, 0.42 M NaCl, 0.2 mM EDTA, 1.5 mM $MgCl_2$, 0.5% v/v Nonidet P-40, 1 mM DTT, 1 mM NaF, 1 mM Na_3VO_4, and 1× complete protease inhibitor cocktail (Roche Diagnostics). The lysates

were frozen and thawed twice and clarified by centrifugation at 12000 rpm for 10 min at 4°C. Protein concentration in each sample was determined using the Bradford colorimetric assay (Bio-Rad Laboratories) and the DU-640 UV Spectrophotometer (Beckman Coulter). The protein samples (20–30 μg total proteins) were electrophoresed through 10% SDS-PAGE, and then transferred to nitrocellulose or PVDF membranes (Bio-Rad Laboratories) for immunoblotting. Primary antibodies against phospho-IGF1R β (1:2000; cat. n. 3024 Cell Signaling Technology), total IGF1R β (1:2000; cat. n. 3027 Cell Signaling Technology), phospho-Akt (Ser473) (1:2000; cat. n. 9271 Cell Signaling Technology), total Akt (1:2000; cat. n. 9272 Cell Signaling Technology), phospho-p44/42 (ERK1/2) (1:2000; cat. n. 9101 Cell Signaling Technology), total p44/42 (ERK1/2) (1:2000; cat. n. 9102 Cell Signaling Technology), PCNA (1:5000, cat. n. MAB 424R Millipore), MF20 (1:500, DSHB), and mouse/rat biotinylated IGF-1 antibody (1:300, cat. n. BAF791 R&D Systems) were incubated overnight at 4°C. For lectin blotting, membranes were probed with biotinylated Concanavalin A (Con A, 1:1000), Phaseolus vulgaris leucoagglutinin (PHA-L, 1:200), and Aleuria Aurantia (AAL, 1:400) lectins (Vector laboratories, D.B.A. Italia) at room temperature while shaking for 1 h. After washes, the membranes were incubated with the appropriate horseradish peroxidase (HRP)-conjugated secondary antibody (against primary antibodies) or streptavidin-HRP (for IGF-1 and biotinylated lectins) at room temperature for 1 h and were then washed three times. Deglycosylation of TA and EDL muscle proteins was performed by incubation tissue lysates with 2.5 U of PNGase F (Sigma-Aldrich; cat. num. P7367) for 2 h at 37°C, according to the manufacturer's recommendations. An aliquot of tissue lysates incubated with an equal volume of PNGase assay reaction buffer without the enzyme PNGase F was used as a control. Blots were developed using Clarity Western ECL Substrate (Bio-Rad Laboratories) and were quantified using the ChemiDoc MP (Bio-Rad Laboratories) equipped with Image Lab software.

2.8 | CRISPR-CTR and CRISPR-PMM2 cellular senescence quantification

Cellular senescence was evaluated via detection of the SA-βgal activity in CRISPR-CTR and CRISPR-PMM2 cells. Wild-type cells were also treated with 600 μM hydrogen peroxide (H_2O_2) for 2 h and served as a positive control.[33] Myoblasts at 80%–90% confluence were washed twice with PBS, fixed for 5 min at room temperature with 4% paraformaldehyde, and washed again three times in PBS. Cells were then incubated overnight at 37°C without CO_2 with freshly prepared staining solution at pH 6 according to Chen et al.[33] After the incubation, six random images per well (10× objective) were collected using a digital camera (ColorView, Soft Imaging Systems) adapted to an inverted microscope (Olympus CKX41). The senescent cells responding to the SA-βgal activity (identified by a blue ring usually around the nucleus) were manually counted with the ImageJ software, and the ratio of senescent cells was calculated.

2.9 | Statistical analysis

Sample size for cell culture experiments was determined based on practicability and prior experience with the C2C12[31] and L6E9[30] cells. The numbers of mice to be used were derived from a power analysis conducted using preliminary data for lectin binding (mean ± SD) in WT mice treated with TUN and considering 80% power an alpha level of significance of .05. Data are represented as mean ± SD of at least three independent experiments. The biological replicate numbers are indicated as the n numbers in the figure legends. Variables of interest were checked for normal distribution using the Shapiro–Wilks test, and parametric statistical analysis was employed to determine significant differences. Results for mRNA expression of *myogenin*, *Mrf4*, *Chop*, *Hspa5*, and *s/uXBP1* ratio were not normally distributed and therefore log-transformed and reanalyzed. Statistical analyses were performed using Student's *t*-test or two-way ANOVA as appropriate, followed by Tukey's multiple comparison post hoc tests. A p-value $<.05$ was considered statistically significant.

3 | RESULTS

3.1 | TUN treatment and C2C12 myoblast differentiation

To mimic a mild CDG-like phenotype, we first aimed to find the minimal dose of TUN for C2C12 myoblasts that would interfere with glycosylation while maintaining cell viability. The optimal TUN treatment of C2C12 myoblasts was established to be 0.01 μg/mL since cells retained the capacity to exclude trypan blue (cytotoxicity CTR = 1.7% ± 1.8%; TUN 0.01 μg/mL for 72 h = 1.8% ± 0.5; $p = .92$) for up to 72 h. At the highest concentration (0.05 μg/mL), cytotoxic effects became apparent, and the myoblasts appeared highly vacuolated and started to detach from the dish surfaces (cytotoxicity CTR = 1.7% ± 1.8%; TUN 0.05 μg/mL for 72 h = 50.5% ± 3.3%; $p < .0001$). Thus, a concentration of 0.01 μg/mL was used to evaluate the effect of chronic low-dose TUN treatment on C2C12. TUN was added to proliferating C2C12 myoblasts 24 h before and during 6 days of cell differentiation. Cells were harvested on days 1 and 6 after the induction of differentiation. First, we used Con A, PHA-L, and AAL lectins to

analyze the glycosylation pattern of C2C12 (Figures 1A and S1A). Con A recognizes oligomannose and hybrid glycans mannose, PHA-L recognizes complex-type N-glycans, while AAL binds to fucose linked (α -1,6) to N-acetylglucosamine or to fucose linked (α -1,3) to N-acetyllactosamine. As shown in Figure 1A, we found a significant increase in Con A, PHA-L, and AAL reactivity at day 6 compared to day 1, indicating a rise in high mannose, complex N-glycans, and fucosylated proteins, respectively. Notably, the lectin binding profile of TUN-treated cells was similar to CTR at day 1 but markedly differed at day 6, showing a general reduction of N-glycosylation. The expression level of ER-stress-related genes *Chop* and *Hspa5* and the *s/uXBP1* ratio increased after TUN treatment at both days 1 and 6 compared to CTR, as expected (Figure 1B). Subsequently, we analyze the effect of TUN treatment on C2C12 differentiation by immunofluorescence analysis of the myosin heavy chain (MF20) (Figure 1C). CTR cells appeared as long multinucleated cells at day 6 (fusion index of 53.8 ± 8.0%), while myotube formation was markedly inhibited in TUN-treated cells (fusion index at day 6 = 18.2 ± 10.7%). We then examined the mRNA levels of myogenic markers *Ccnd1*, *MyoD*, *myogenin*, and *Mrf4* during differentiation (Figure 1D). In CTR cells, *Ccnd1* was expressed on day 1 and was downregulated on day 6, as expected. *MyoD* and *myogenin* showed the opposite trend. In TUN-treated cells, *Ccnd1* was not downregulated on day 6 but appeared to increase. In addition, TUN-treated cells expressed significantly lower levels of *MyoD*, *myogenin*, and *Mrf4* mRNAs compared to CTR on days 1 and 6. Finally, we found that TUN treatment increased the PCNA protein expression on day 1 and markedly reduced the MF20 protein expression compared to CTR on day 6 (Figure 1E,F). We found that TUN treatment inhibited the differentiation (Figure S2A), increased *Ccnd1* mRNA expression on day 1, and decreased *MyoD*, *myogenin*, and *Mrf4* mRNA levels on day 4 (Figure S2B) of rat L6E9 myoblasts, similar to C2C12 myoblasts, which indicate that N-glycosylation has a crucial role in myoblast differentiation.

3.2 | PMM2 knockdown and C2C12 myoblast differentiation

Subsequently, we knocked down *PMM2* in C2C12 by stable transfection of *PMM2* CRISPR/Cas9 double-nickase plasmid to analyze the effects of PMM2 deficiency on myoblast

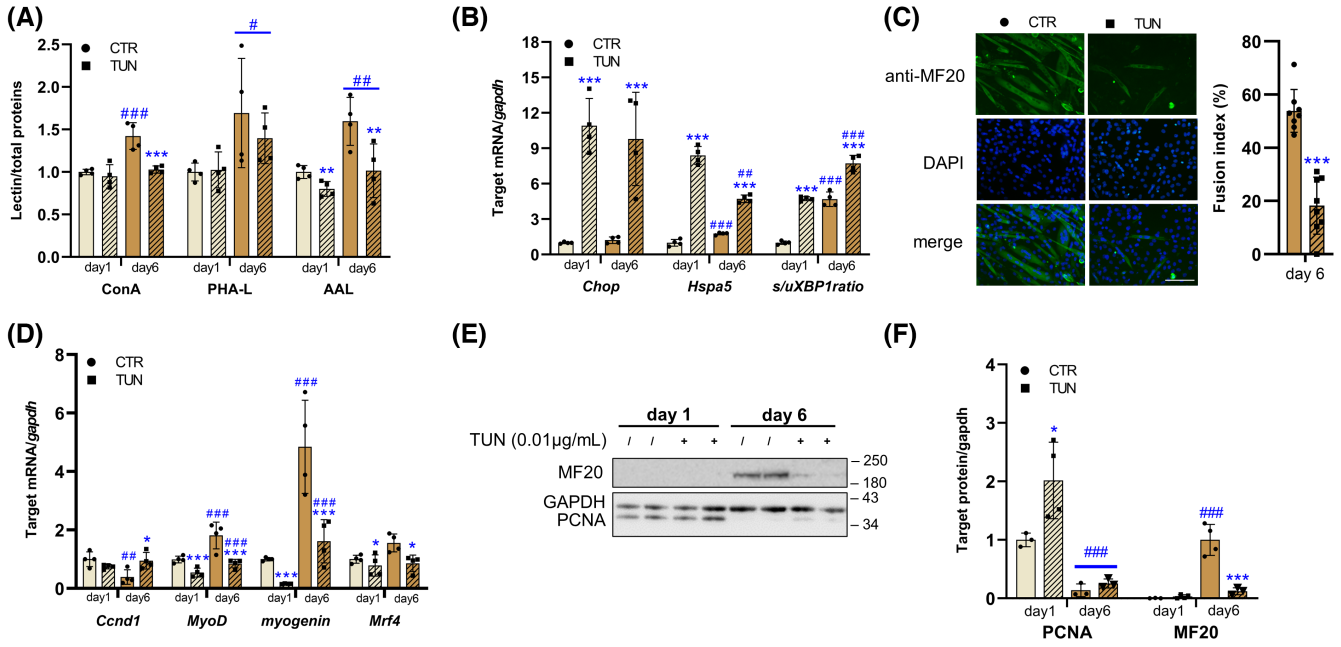

FIGURE 1 Effect of TUN treatment on C2C12 cell differentiation. (A) Quantification of lectin binding in C2C12 treated with TUN (0.01 μg/mL); C2C12 cells were collected on days 1 and 6 ($n = 4$). AAL, *Aleuria aurantia* lectin; ConA, concanavalin A; PHA-L, *Phaseolus vulgaris* leucoagglutinin. Representative lectin blots were presented in Figure S1A. (B) Expression of ER-stress-related genes *Chop*, *Hspa5*, and *s/uXBP1* ratio in C2C12 cells treated with TUN (0.01 μg/mL) ($n = 4$). (C) Effects of TUN treatment (0.01 μg/mL) on myotubes formation at day 6 ($n = 8$), the scale bar represents 100 μm. (D) Quantification of *Ccnd1*, *MyoD*, *myogenin*, and *Mrf4* mRNA expression by qRT-PCR ($n = 4$). (E) Representative immunoblotting and (F) band densitometry analysis of C2C12 treated with 0.01 μg/mL of TUN using antibodies directed against PCNA and MF20. All bar charts are presented as mean values ± SD. Significant differences were determined using unpaired *t*-test (C) or two-way ANOVA followed by Tukey's multiple comparison post hoc tests (A, B, D, F). *Significantly different compared to CTR; #Significantly different compared to day 1; * and # $p \leq .05$; ** and ## $p \leq .01$, *** and ### $p \leq .001$.

differentiation. RNA from PMM2-targeted cells (CRISPR-PMM2) and control plasmid-transfected cells (CRISPR-CTR) was collected to confirm the effective targeting of the *PMM2* gene. We obtained three myoblast clones with a marked reduction in *PMM2* mRNA expression compared with the corresponding CRISPR-CTR clones (10.7 ± 2.8 fold reduction at day 1; $p < .0001$). Accordingly, CRISPR-PMM2 myoblasts had a significantly reduced PMM enzyme activity (CRISPR-CTR at day 1 = 1.64 ± 0.4 mU/mg of proteins; CRISPR-PMM2 at day 1 = 0.34 ± 0.25 mU/mg of proteins; $p < .01$) and the downregulation of *PMM2* mRNA expression also persisted in cells harvested at day 6 after differentiation (16.9 ± 4.0 fold reduction; $p < .0001$). The lectin binding profile of CRISPR-PMM2 cells showed a reduction of lectins binding at day 6 compared to CRISPR-CTR (Figures 2A and S1B). The analyses of the expression level of ER-stress-related genes in CRISPR-PMM2 cells showed a slight increase of *s/uXBP1* ratio on day 1 and a marked increase of *Chop* and *Hspa5* mRNA level and *s/uXBP1* ratio on day 6 compared to CRISPR-CTR (Figure 2B). We next examined the differentiation potential of CRISPR-PMM2 myoblasts. As shown in Figure 2C, CRISPR-PMM2 cells failed to form myotubes at day 6, showing a marked reduction in the myogenic index (CRISPR-CTR fusion index at day 6 = 51.0 ± 8.7%; CRISPR-PMM2 fusion index at day 6 = 0.9 ± 0.6%) (Figure 2C). We found an increase of *Ccnd1* mRNA and decrease *MyoD* and *myogenin* mRNA levels in CRISPR-PMM2 at day 1 compared to CRISPR-CTR cells (Figure 2D), while the PCNA protein expression did not change (Figure 2E,F). Conversely, *MyoD*, *myogenin*, and *Mrf4* mRNA levels (Figure 2D) and MF20 protein expression (Figure 2E,F) strongly decreased at day 6. The analysis of senescence-associated beta-galactosidase (SA-βgal) activity showed no difference between CRISPR-PMM2 and CRISPR-CTR myoblast (% senescence CRISPR-CTR = 2.5 ± 2.4; CRISPR-PMM2 = 2.2 ± 2.1; $p = .85$), suggesting that the lack of differentiation cannot be attributed to senescence in the selected CRISPR-PMM2 clones.

3.3 | Effects of chronic treatment with low TUN dose on TA muscle lectin binding, ER-stress-related gene expression, and muscle markers of myogenesis and atrophy

To investigate the role of N-glycosylation inhibition on muscle *in vivo*, 6-week-old WT and MLC/mIgf-1

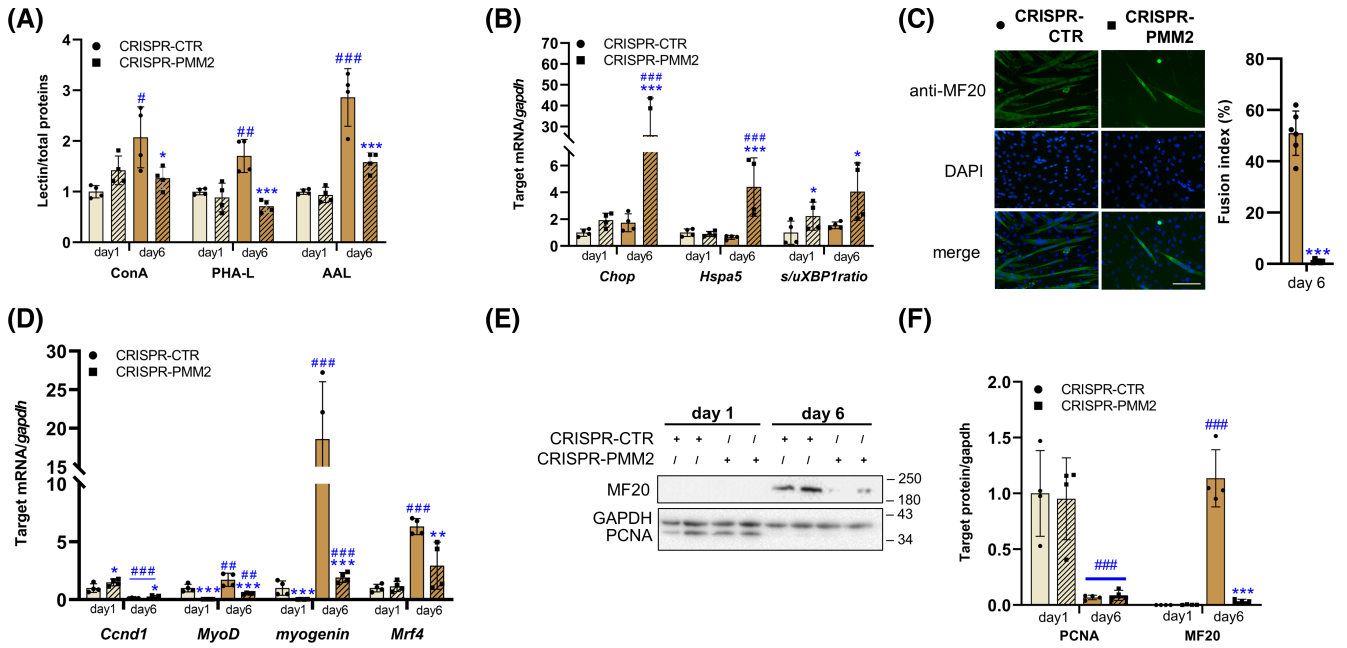

FIGURE 2 Effect of PMM2 downregulation on C2C12 differentiation. (A) Quantification of lectin binding after knockdown of *PMM2* gene by CRISPR/Cas9 (CRISPR-PMM2) and control plasmid-transfected cells (CRISPR-CTR). AAL, *Aleuria aurantia* lectin; ConA, concanavalin A; PHA-L, *Phaseolus vulgaris* leucoagglutinin. Representative lectin blots were presented in Figure S1B. (B) Expression of ER-stress-related genes *Chop*, *Hspa5*, and *s/uXBP1* ratio in CRISPR-CTR and CRISPR-PMM2 C2C12; C2C12 cells were collected on days 1 and 6 ($n = 4$). (C) Effects of PMM2 knockdown on myotubes formation at day 6 ($n = 6$), the scale bar represents 100 μm. (D) Quantification of *Ccnd1*, *MyoD*, *myogenin*, and *Mrf4* mRNA expression by qRT-PCR ($n = 4$). (E) Representative immunoblotting and (F) band densitometry analysis of CRISPR-CTR and CRISPR-PMM2 C2C12 using antibodies directed against PCNA and MF20. All bar charts are presented as mean values ± SD. Significant differences were determined using unpaired *t*-test (C) or two-way ANOVA followed by Tukey's multiple comparison post hoc tests (A, B, D, F). *Significantly different compared to CTR; #Significantly different compared to day 1; * and # $p \leq .05$; ** and ## $p \leq .01$, *** and ### $p \leq .001$.

mice were chronically challenged with a low TUN dose (0.1 mg/kg for 15 days). MLC/mIgf-1 mice showed increased body and TA muscle weight compared to WT mice (Figure 3A), as expected.[29] Conversely, body and TA muscle weight were similar between CTR and TUN-treated mice (Figure 3A). TUN treatment decreased ConA lectin binding in the TA muscle of WT and MLC/mIgf-1 mice, while AAL reactivity markedly decreased only in TA muscle of WT mice (Figures 3B and S1C). The ER-stress-related gene expression did not change in the TA muscle of WT and MLC/mIgf-1 mice (Figure 3C). In TA muscle of WT and MLC/mIgf-1 mice, the mRNA expression of *myogenin* decreased after TUN treatment, while *atrogin-1* expression levels increased only in the WT mice (Figure 3D).

3.4 | Effects of chronic treatment with low TUN dose on *Igf-1* mRNA and IGF-1 protein expression and on IGF1R pathways activation in the TA muscle of WT and MLC/mIgf1 mice and in C2C12 myoblasts

The expression of endogenous *Igf-1Ea* and *Igf-1Ec* isoforms slightly decreased after TUN treatment in TA (Figure 4A) and EDL (Figure S3A) muscle of WT and MLC/mIgf1 mice, although this reduction was statistically significant only in TA muscle. We also measured the effect of TUN treatment on the expression of *mIgf-1* transgene by quantifying total *Igf-1* (*Igf-1tot*) mRNA. It is important to note that the primer set used to amplify the expression of *mIgf-1* transgene (i.e., *Igf-1 tot*)

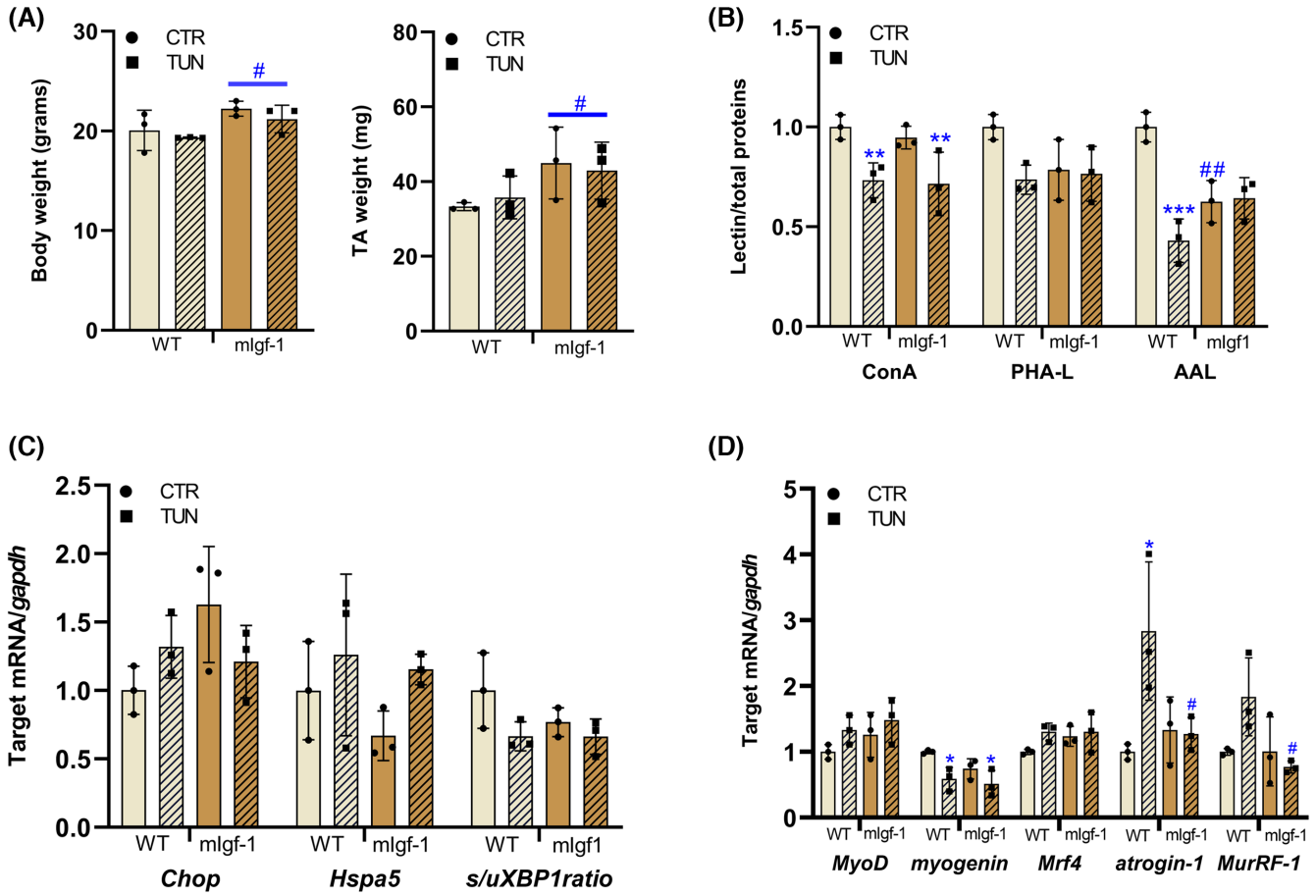

FIGURE 3 Effect of chronic treatment with low TUN dose (0.1 mg/kg of TUN for 15 days) on TA muscle of WT and MLC/mIgf-1 mice. (A) Body and TA muscle weight of WT ($n = 3$) and MLC/mIgf-1 ($n = 3$) mice treated with TUN for 15 days. (B) Quantification of lectin binding in the TA muscle of WT ($n = 3$) and MLC/mIgf-1 ($n = 3$) mice treated with TUN; AAL, *Aleuria aurantia* lectin; ConA, concanavalin A; PHA-L, *Phaseolus vulgaris* leucoagglutinin. Representative lectin blots were presented in Figure S1C. (C) Expression of ER-stress-related genes *Chop* and *Hspa5* and *s/uXBP1* ratio in the TA muscle of WT ($n = 3$) and MLC/mIgf-1 ($n = 3$) mice treated with TUN. (D) Quantification of *MyoD*, *myogenin*, *Mrf4, atrogin-1*, and *MuRF-1* mRNA expression by qRT-PCR in the TA muscle of WT ($n = 3$) and MLC/mIgf-1 ($n = 3$) mice treated with TUN ($n = 3$). All bar charts are presented as mean values ± SD. Significant differences were determined using two-way ANOVA followed by Tukey's multiple comparison post hoc tests. *Significantly different compared to CTR; #Significantly different compared to WT mice; * and # $p \leq .05$; ** and ## $p \leq .01$, ***$p \leq .001$.

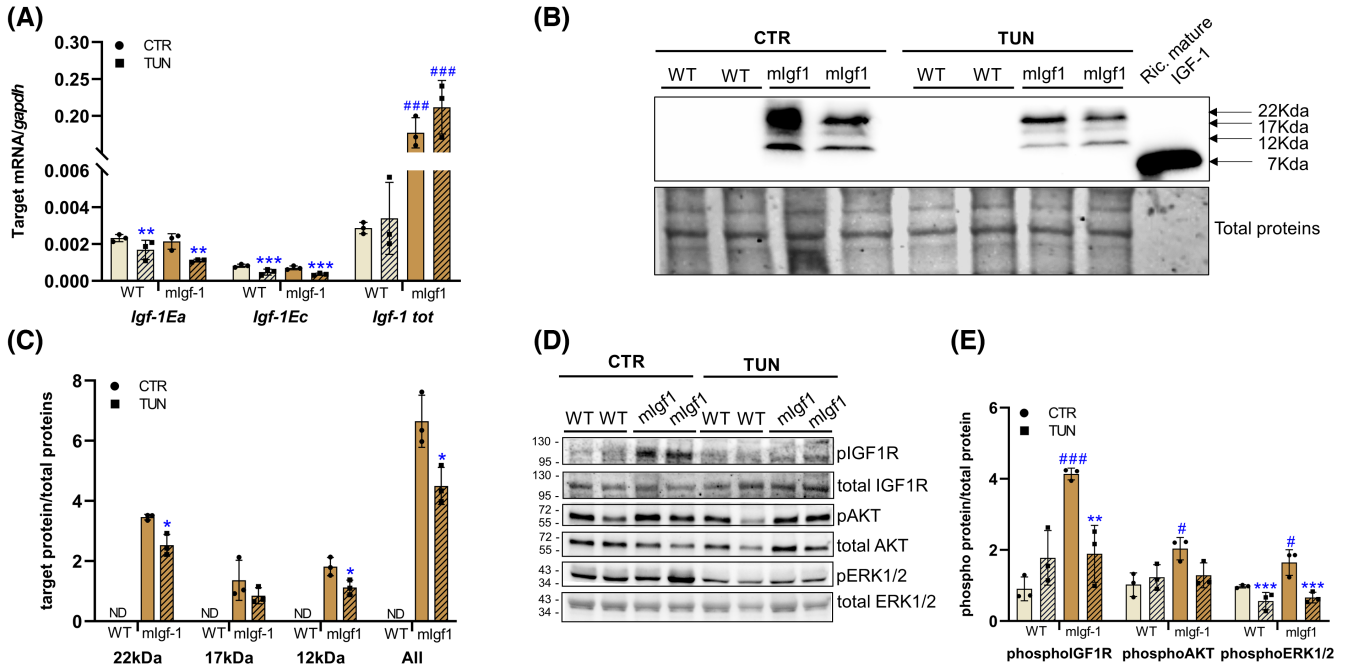

FIGURE 4 IGF-1 production and IGF1R signaling pathway activation in TA muscle of WT and MLC/mIgf-1 mice treatment with low TUN dose (0.1 mg/kg of TUN for 15 days). (A) Expression of endogenous *Igf-1* mRNA isoforms (i.e., *Igf-1Ea* and *Igf-1Ec* mRNAs) and total *Igf-1* (i.e., endogenous and mIgf-1 transgene mRNAs) in the TA muscle of WT ($n = 3$) and MLC/mIgf-1 ($n = 3$) mice treated with TUN. (B) Representative immunoblotting and (C) band densitometry analysis of TA muscle of WT and MLC/mIgf1 mice using an antibody directed against mature mouse IGF-1 sequence. Three bands at a molecular weight of ~22, ~17, and ~12 kDa were detected in TA muscle of MLC/mIgf1 mice. Recombinant mouse IGF-1 mature protein was loaded as a positive control for mature IGF-1 (~7 kDa). (D) Representative immunoblotting and (E) band densitometry analysis of TA muscle of WT and MLC/mIgf1 mice using antibodies directed against phosphorylated (pIGF1R) and total IGF1R, phosphorylated (pAKT) and total AKT, and phosphorylated (pERK1/2) and total ERK1/2. All bar charts are presented as mean values ± SD. Significant differences were determined using unpaired *t*-test (C) or two-way ANOVA followed by Tukey's multiple comparison post hoc tests (A, E). *Significantly different compared to CTR; #Significantly different compared to WT mice; * and # $p \leq .05$; ** $p \leq .01$ *** and ### $p \leq .001$.

also recognizes the endogenous *Igf-1* mRNA isoforms (i.e., *Igf-1Ea* and *Igf-1Ec* mRNAs). However, the *mIgf-1* transgene is highly expressed compared to the endogenous *Igf-1* gene ($2^{-\Delta\Delta CT} = 59.5 \pm 10.5$), and hence the *Igf-1Ea* and *Igf-1Ec* mRNA quantity was negligible compared to that of *mIgf-1* transgene. Interestingly, we found that the *mIgf-1* transgene was unaffected by the TUN treatment in the TA (Figure 4A) and EDL (Figure S3A) muscles of MLC/mIgf1 mice. Western blot analyses showed that the TA (Figure 4B) and EDL (Figure S3B) muscles of untreated MLC/mIgf1 mice mainly expressed IGF-1Ea prohormones with three immunoreactive bands of ~22, ~17, and ~12 kDa. The ~22 and ~17 kDa bands disappeared after the deglycosylation with PNGase F, resulting in an accumulation of the ~12 kDa band (Figure S4). Thus, the ~22 and ~17 kDa bands likely represent two N-glycosylated forms of the IGF-1Ea prohormone, while the lower band of ~12 kDa represents the unglycosylated IGF-1Ea prohormone. No IGF-1 immunoreactive signals were detected in the TA and EDL muscles of WT mice, probably because the amount of IGF-1 was below the detection limit of Western blot. Band densitometry analysis showed that TUN treatment decreased the 22 and 12 kDa bands in the TA muscle (Figure 4C) and those of 17 and 12 kDa in the EDL muscle (Figure S3C) of MLC/mIgf-1 mice. Finally, TA muscle of MLC/mIgf1 mice showed increased IGF1R phosphorylation compared to WT mice, which was markedly inhibited by TUN treatment (Figure 4D,E). Accordingly, AKT and MAPK ERK1/2 phosphorylation in the TA muscle of WT and MLC/mIgf1 mice decreased after TUN treatment. Similar results were obtained in the EDL muscle of WT and MLC/mIgf1 mice (Figures S3D,E). The effect of TUN treatment on IGF1R signaling pathway was also investigated on C2C12 harvested on day 1 (Figure 5). Interestingly, we found a marked reduction of total IGF1R and increased mobility shift of IGF1R proreceptor in TUN-treated cells (Figure 5A), suggesting that TUN treatment altered the IGF1R proreceptor processing and total IGF1R quantity, as previously described.[8,11] Subsequently, we analyzed the sub-cellular localization of IGF1R by immunofluorescence staining (Figure 5B).

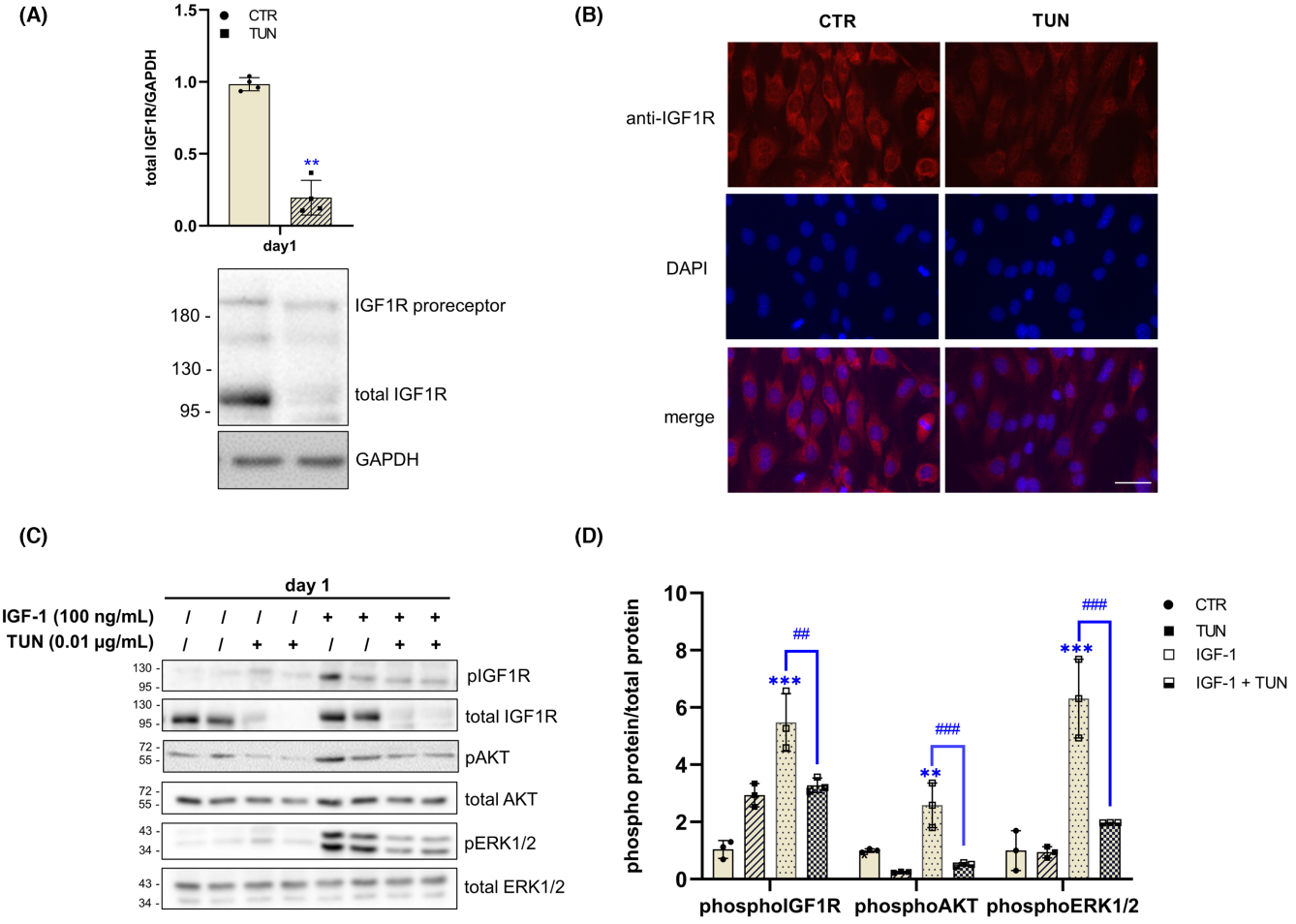

FIGURE 5 Effect of TUN treatment on IGF1R production and IGF1R signaling pathway activation in C2C12. (A) IGF1R and IGF1R proreceptor production in C2C12 cells treated with 0.01 µg/mL of TUN and harvested at day 1. (B) Immunofluorescence analysis of C2C12 cells stained with ant-IGF1R and DAPI, the scale bar represents 200 µm. (C) Representative immunoblotting and (D) band densitometry analysis of IGF-1-induced IGF-1R signaling pathway activation in CTR- and TUN-treated C2C12 cells using antibodies directed against phosphorylated (pIGF1R) and total IGF1R, phosphorylated (pAKT) and total AKT, and phosphorylated (pERK1/2) and total ERK1/2. The calculation of pIGF1R level was normalized against total lysed protein instead of total IGF1R to account for the marked reduction of total IGF1R after TUN treatment. All bar charts are presented as mean values ± SD. Significant differences were determined using unpaired *t*-test (A) or one-way ANOVA followed by Tukey's multiple comparison post hoc tests (D). *Significantly different compared to CTR, #Significantly different compared to IGF-1-treated cells; ** $p \leq .01$, *** $p \leq .001$; ## $p \leq .01$, ### $p \leq .001$.

C2C12 CTR cells showed mainly perinuclear and diffuse cytoplasmic pattern, which was markedly reduced after TUN treatment. Altogether, these results showed that N-glycosylation inhibition affects the IGF1R signaling pathway activation due to the reduction of IGF-1 production and IGF1R activity. To evaluate if IGF1R reduction observed after TUN treatment was associated with reduced IGF1R signaling pathway activation, C2C12 were treated with recombinant mouse IGF-1 (100 ng/mL) for 30 min, and the level of IGF1R, AKT, and MAPK ERK1/2 phosphorylation was quantified by Western blotting (Figure 5C,D). This analysis demonstrated that the IGF-1-induced activation of IGF1R signaling pathway was markedly reduced in TUN-treated C2C12 compared to CTR cells.

4 | DISCUSSION

In this study, we used two *in vitro* strategies to study the effects of N-glycosylation inhibition on C2C12 myoblast differentiation, one based on TUN treatment and one based on PMM2 downregulation. Chronic treatment with a low dose of TUN, intended to prompt a mild impairment of N-glycosylation resembling a mild CDG phenotype, was also administrated in WT and MLC/mIgf-1 mice in order to investigate the effects of N-glycosylation inhibition on muscle *in vivo*. TUN is an inhibitor of DPAGT1 at the first step in the N-glycosylation pathway and prompts a deficiency of N-linked glycans.[34] TUN is also an ER-stress activator due to the accumulation of hypoglycosylated and misfolded proteins.[35] In untreated C2C12 cells, we

observed an increased binding of ConA, PHA-L, and AAL lectins during myoblast differentiation. This finding is in keeping with other studies and suggests that muscle cell glycosylation changes during differentiation.[19,20] A comparison of differentiated and undifferentiated C2C12 cells shows that glycoproteins derived from myotubes bear higher oligomannose/hybrid-type N-glycan (ConA), complex-type N-glycan (PHA-L), and fucosylated (AAL) residues. Interestingly, C2C12 cells differentiated under TUN treatment exhibited a lectin binding pattern more similar to the undifferentiated myoblasts. We found an increase in ER-stress-related gene expression (*Chop* and *Hspa5* mRNAs and *s/uXbp1* ratio) in C2C12 myoblast and myotubes treated with TUN compared to those untreated, as expected. Interestingly, TUN-induced hypoglycosylation decreased myogenic markers and prevented myotubes formation in C2C12. Previous studies have shown that doses from 1.0 to 10 μg/mL of TUN are toxic in C2C12 cells, induce strong ER-stress pathways activation, inhibit mitosis, and increase apoptosis.[36] However, the effects of high TUN dose on myoblast differentiation are still unclear, probably due to its toxicity and off-target effects.[22,36,37] Here, we found that low TUN doses (i.e., concentration ≤ 0.01 μg/mL) do not have toxic effects on C2C12 myoblasts and preserve myoblast proliferation (we observed increased PCNA protein levels). Hence, the inhibition of C2C12 differentiation induced by non-toxic doses of TUN is likely to be caused by the TUN-induced hypoglycosylation instead of unexpected secondary effects (i.e., mitosis arrest and apoptosis) described in other studies.[22,36] To confirm the detrimental effect of hypoglycosylation on myoblast differentiation, we produced C2C12 cells with stable downregulation of *PMM2*. The PMM2 protein is an enzyme that converts mannose-6-phosphate into mannose-1-phosphate, the immediate precursor of GDP-mannose which is a key substrate for the synthesis of glycans. PMM2 is the most frequently mutated enzyme in human CDG. Living PMM2-CDG patients harbor hypomorphic alleles and residual PMM2 activity because the complete loss of PMM2 function is lethal.[38] We found that the PMM2 downregulation decreased lectin binding in myotubes while the ER-stress-related gene expression increased, as expected. Interestingly, the differentiation process and myotube formation were markedly inhibited after PMM2 dowregulation, corroborating results obtained in TUN-treated cells. Nevertheless, CRISPR cells also showed some small differences with respect to C2C12 challenged with TUN and parental WT cell population. In particular, *Chop* and *Hspa5* mRNA levels markedly increased at day 1 and still remained high at day 6 after TUN treatment, whereas these ER-stress markers increased only at day 6 in CRISPR-PMM2 cells. Moreover, the magnitude of relative expression changes of *Chop*, *myogenin*, and *MRF4* mRNAs was higher in CRISPR compared to parental WT cells. A slightly different phenotype between CRISPR C2C12 clonal derivatives and parental cells was expected,[39] although we verified that CRISPR-CTR clones maintain differentiation capability. Moreover, both CRISPR-CTR and CRISPR-PMM2 myoblasts did not show cellular senescence as demonstrated by β-galactosidase assay. An alternative possibility to explain the difference between TUN-treated and CRISPR-PMM2 cells might be related to the disease mechanism behind each model since mutations in *DPAGT1* gene, which encodes the target of TUN, caused the DPAGT1-CDG which is characterized by a more severe clinical phenotypes compared to PMM2-CDG.[40,41] Thus, although both TUN-treated and CRISPR-PMM2 cells showed reduced lectin binding and myoblast differentiation, future efforts should be made to create models that fully mimics the PMM2 mutations found in patients and to investigate the impact of PMM2 deficiency on myogenic differentiation using primary patient-derived myoblasts. PMM2-CDG is associated with a broad range of clinical symptoms including generalized hypotonia, distal muscle atrophy, and wasting also related to peripheral neuropathy. Signs of myopathy can be moderate (6% of patients) to severe (2% of patients) in the natural history of PMM2-CDG.[42] Recently, Muthusamy K et al. demonstrated that about 82% of the 51 patients included in the studied PMM2-CDG population exhibited clinical myopathy, suggesting that myopathy is a commonly overlooked aspect of this disease.[43] Although uncommon in infancy, cardiomyopathy can also occur in PMM2-CDG and represents a life-threatening condition.[44,45] Observation of muscle histology is very rarely described in PMM2-CDG, but mild myopathic changes regarding fiber size variation and myofibrillar disarray have been reported.[46] Mildly elevated serum creatine kinase can also occur.[47] Muscle-specific *PMM2* knockdown causes qualitative movement defects in *Drosophila*.[48] Although the pathophysiology of hypotonia in PMM2-CDG is probably complex, our results suggest that the hypoglycosylation-induced defective differentiation of myoblasts into myotubes could be a contributing factor.

Xia et al. recently demonstrated that a chronic administration of TUN to C57BL/6 mice induces growth retardation (reduced weight, height, and tibia length) in association with low IGF-1 production and signaling.[23] Moreover, it has been shown that N-glycosylation has an essential function in protein folding, stability, and intracellular trafficking of both IGF-1 prohormone and IGF1R proreceptor.[5,6,49] Low IGF1R expression in primary fibroblasts derived from CDG patients with deficient N-glycosylation[49,50] and in HEK293 cells lacking the catalytically active subunit of the Oligosaccharyltransferase (OST)[6] has been shown. Furthermore, desialylation of

IGF1R decreased the proliferative response of L6 myoblasts[51] and receptor activity in a cell model of GNE myopathy.[52] We therefore evaluated the IGF-1 signaling pathway activation in TA and EDL muscles of WT and MLC/mIgf-1 transgenic mice treated with chronic (15 days) low dose of TUN. We found that TUN reduced ConA lectin reactivity in TA muscle from WT and MLC/mIgf-1 mice and AAL binding in MLC/mIgf-1 mice. ER-stress-related gene expression did not change in the TA muscle of WT and MLC/mIgf-1 mice. Since continuous low-dose administration of TUN has a relatively mild impact on glycosylation and ER-stress marker expression, we can suppose that this condition resembles a mild CDG phenotype. The myogenic marker *myogenin* was downregulated in the TA muscles of WT and MLC/mIgf-1 mice after low-dose TUN treatment. Moreover, the mRNA expression of muscle atrophy marker *atrogin-1* was increased in WT mice after TUN treatment. Interestingly, we found a slight reduction of endogenous *Igf-1Ea and Igf-1Ec* mRNA isoforms in association with TUN administration in TA muscle of both WT and MLC/mIgf-1 mice; however, this decrease did not reach statistical significance in EDL muscle. Moreover, *mIgf-1* transgene overexpression in MLC/mIgf-1 mice did not change after TUN treatment. Thanks to the overexpression of *Igf-1Ea* in the MLC/mIgf-1 mice, we were also able to analyze the impact of TUN on muscle IGF-1Ea proteins by Western blot. Muscle IGF-1 was mainly expressed as proIGF-1Ea not mature IGF-1, as previously shown.[5,10] The expression level of proIGF-1Ea, including the ~22 kDa band, likely representing an N-glycosylated form of proIGF-1Ea,[5,10,49] decreased after TUN treatment. IGF1R and AKT activation were reduced after TUN treatment in the muscle of MLC/mIgf-1 mice while both WT and MLC/mIgf-1 mice showed reduced MAPK ERK1/2 phosphorylation compared to untreated mice. The reduction of IGF-1 prohormone production and IGF1R signaling pathway activation was also observed in EDL muscle of WT and MLC/mIgf-1 mice treated with TUN. Moreover, using C2C12 myoblasts, we demonstrated reduced IGF1R expression and increased IGF1R proreceptor mobility shift after TUN treatment, which was associated with marked reduction of IGF1R, AKT, and MAPK ERK1/2 activation following exogenous IGF-1 treatment. Given the important role played by the IGF1R signaling pathway on myoblast proliferation and muscle cell growth,[3,53] our results suggested that reduced IGF1 production and IGF1R signaling activation may be involved in the impaired muscle development and function found in CDG. However, the molecular effectors underlying the pathophysiology of muscle involvement in CDG are only starting to be unraveled, and further studies are needed to clarify the involved biological pathways. In this regard, chronic TUN-challenge mouse models can help elucidate the molecular mechanisms through which diseases associated with aberrant N-glycosylation, differentially affect tissue, and organ function.

AUTHOR CONTRIBUTIONS

Giosuè Annibalini and Elena Barbieri: Conceptualization, Formal analysis, Funding acquisition, Resources, Data curation, Writing – Reviewing and Editing; Laura Di Patria, Giacomo Valli, Matteo Bocconcelli, and Fabiana Fanelli: Investigation, Visualization; Roberta Saltarelli, Lorenzo Ferri, and Laura Barberi Investigation, Visualization, Writing – Original draft preparation; Amelia Morrone, Rita Barone, Renzo Guerrini, Antonio Musarò, and Vilberto Stocchi: Supervision, Funding acquisition, Resources, Writing – Reviewing and editing. All the authors contributed to manuscript revision, and read and approved the submitted version.

ACKNOWLEDGMENTS

This study is funded by the European Union—Next Generation EU (PRIN 2022; project n. 202255RLB4 and n. 2022LZARA3) and from the University of Urbino Carlo Bo "Promozione della salute e della sicurezza alimentare" (D.R. 446/2020), AFM-Telethon (Project n. 23608) and Fondazione Roma 2022/2025. We gratefully thank the AMMeC (Associazione Malattie Metaboliche e Congenite, Italia). The authors acknowledge the support of NBFC to AM, funded by the National Recovery and Resilience Plan (NRRP), Mission 4 Component 2 Investment 1.4.

DISCLOSURES

None of the authors have any conflicts of interest or financial ties to disclose.

DATA AVAILABILITY STATEMENT

The data that support the findings of this study are available in the methods and/or supplementary material of this article.

ORCID

Giosuè Annibalini https://orcid.org/0000-0002-6914-4905
Laura Di Patria https://orcid.org/0000-0002-1859-6928
Giacomo Valli https://orcid.org/0000-0002-5221-580X
Matteo Bocconcelli https://orcid.org/0009-0004-0648-9764
Roberta Saltarelli https://orcid.org/0000-0002-6375-127X
Lorenzo Ferri https://orcid.org/0000-0001-5740-5429
Laura Barberi https://orcid.org/0000-0002-7671-4750
Fabiana Fanelli https://orcid.org/0009-0009-6465-2909
Amelia Morrone https://orcid.org/0000-0003-2890-8179
Rita Barone https://orcid.org/0000-0001-6302-2686
Renzo Guerrini https://orcid.org/0000-0002-7272-7079
Antonio Musarò https://orcid.org/0000-0002-2944-9739
Vilberto Stocchi https://orcid.org/0000-0003-3269-9410
Elena Barbieri https://orcid.org/0000-0002-3480-7983

REFERENCES

1. Bentzinger CF, Wang YX, Rudnicki MA. Building muscle: molecular regulation of myogenesis. *Cold Spring Harb Perspect Biol*. 2012;4:a008342.
2. Kislinger T, Gramolini AO, Pan Y, Rahman K, MacLennan DH, Emili A. Proteome dynamics during C2C12 myoblast differentiation. *Mol Cell Proteomics*. 2005;4:887-901.
3. Yoshida T, Delafontaine P. Mechanisms of IGF-1-mediated regulation of skeletal muscle hypertrophy and atrophy. *Cells*. 2020;9:1970.
4. Glass DJ. PI3 kinase regulation of skeletal muscle hypertrophy and atrophy. *Curr Top Microbiol Immunol*. 2010;346:267-278.
5. Annibalini G, Contarelli S, De Santi M, et al. The intrinsically disordered E-domains regulate the IGF-1 prohormones stability, subcellular localisation and secretion. *Sci Rep*. 2018;8:8919.
6. Klaver E, Zhao P, May M, et al. Selective inhibition of N-linked glycosylation impairs receptor tyrosine kinase processing. *Dis Model Mech*. 2019;12:dmm039602.
7. Siddals KW, Marshman E, Westwood M, Gibson JM. Abrogation of insulin-like growth factor-I (IGF-I) and insulin action by mevalonic acid depletion. *J Biol Chem*. 2004;279:38353-38359.
8. Itkonen HM, Mills IG. N-linked glycosylation supports cross-talk between receptor tyrosine kinases and androgen receptor. *PLoS ONE*. 2013;8:e65016.
9. Luo YE, Villani KR, Lei H, et al. Ablation of specific insulin-like growth factor I forms reveals the importance of cleavage for regenerative capacity and glycosylation for skeletal muscle storage. *FASEB J*. 2024;38:e23634.
10. Durzyńska J, Philippou A, Brisson BK, Nguyen-McCarty M, Barton ER. The pro-forms of insulin-like growth factor I (IGF-I) are predominant in skeletal muscle and alter IGF-I receptor activation. *Endocrinology*. 2013;154:1215-1224.
11. Dricu A, Kanter L, Wang M, et al. Expression of the insulin-like growth factor 1 receptor (IGF-1R) in breast cancer cells: evidence for a regulatory role of dolichyl phosphate in the transition from an intracellular to an extracellular IGF-1 pathway. *Glycobiology*. 1999;9:571-579.
12. Pucci M, Venturi G, Malagolini N, Chiricolo M, Dall'Olio F. Glycosylation as a main regulator of growth and death factor receptors signaling. *Int J Mol Sci*. 2018;19:580.
13. Vergé C, Bouchatal A, Chirat F, Guérardel Y, Maftah A, Petit J. Involvement of ST6Gal I-mediated α2,6 sialylation in myoblast proliferation and differentiation. *FEBS Open Bio*. 2020;10:56-69.
14. Janot M, Audfray A, Loriol C, Germot A, Maftah A, Dupuy F. Glycogenome expression dynamics during mouse C2C12 myoblast differentiation suggests a sequential reorganization of membrane glycoconjugates. *BMC Genomics*. 2009;10:483.
15. Grassot V, Da Silva A, Saliba J, Maftah A, Dupuy F, Petit J-M. Highlights of glycosylation and adhesion related genes involved in myogenesis. *BMC Genomics*. 2014;15:621.
16. Martin PT. Glycobiology of neuromuscular disorders. *Glycobiology*. 2003;13:67R-75R.
17. Blazev R, Ashwood C, Abrahams JL, et al. Integrated glycoproteomics identifies a role of N-glycosylation and galectin-1 on myogenesis and muscle development. *Mol Cell Proteomics*. 2021;20:100030.
18. Gundry RL, Raginski K, Tarasova Y, et al. The mouse C2C12 myoblast cell surface N-linked glycoproteome. *Mol Cell Proteomics*. 2009;8:2555-2569.
19. McMorran BJ, McCarthy FE, Gibbs EM, et al. Differentiation-related glycan epitopes identify discrete domains of the muscle glycocalyx. *Glycobiology*. 2016;26:1120-1132.
20. McMorran BJ, Miceli MC, Baum LG. Lectin-binding characterizes the healthy human skeletal muscle glycophenotype and identifies disease-specific changes in dystrophic muscle. *Glycobiology*. 2017;27:1134-1143.
21. Godfrey C, Foley AR, Clement E, Muntoni F. Dystroglycanopathies: coming into focus. *Curr Opin Genet Dev*. 2011;21:278-285.
22. Olden K, Law J, Hunter VA, Romain R, Parent JB. Inhibition of fusion of embryonic muscle cells in culture by tunicamycin is prevented by leupeptin. *J Cell Biol*. 1981;88:199-204.
23. Xia W, Wang Y, Zhang Y, et al. Endoplasmic reticulum stress induces growth retardation by inhibiting growth hormone IGF-I axis. *Growth Hormon IGF Res*. 2020;55:101341.
24. Nicolau S, Liewluck T, Shen X-M, Selcen D, Engel AG, Milone M. A homozygous mutation in GMPPB leads to centronuclear myopathy with combined pre- and postsynaptic defects of neuromuscular transmission. *Neuromuscul Disord*. 2019;29:614-617.
25. Freeze HH, Jaeken J, Matthijs G. CDG or not CDG. *J Inherit Metab Dis*. 2022;45:383-385.
26. Péanne R, de Lonlay P, Foulquier F, et al. Congenital disorders of glycosylation (CDG): quo vadis? *Eur J Med Genet*. 2018;61:643-663.
27. Pettinato F, Mostile G, Battini R, et al. Clinical and radiological correlates of activities of daily living in cerebellar atrophy caused by PMM2 mutations (PMM2-CDG). *Cerebellum*. 2021;20:596-605.
28. Serrano M, de Diego V, Muchart J, et al. Phosphomannomutase deficiency (PMM2-CDG): ataxia and cerebellar assessment. *Orphanet J Rare Dis*. 2015;10:138.
29. Musarò A, McCullagh K, Paul A, et al. Localized Igf-1 transgene expression sustains hypertrophy and regeneration in senescent skeletal muscle. *Nat Genet*. 2001;27:195-200.
30. Musarò A, Rosenthal N. Maturation of the myogenic program is induced by postmitotic expression of insulin-like growth factor I. *Mol Cell Biol*. 1999;19:3115-3124.
31. Sestili P, Barbieri E, Martinelli C, et al. Creatine supplementation prevents the inhibition of myogenic differentiation in oxidatively injured C2C12 murine myoblasts. *Mol Nutr Food Res*. 2009;53:1187-1204.
32. Van Schaftingen E, Jaeken J. Phosphomannomutase deficiency is a cause of carbohydrate-deficient glycoprotein syndrome type I. *FEBS Lett*. 1995;377:318-320.
33. Chen J-H, Ozanne SE, Hales CN. Methods of cellular senescence induction using oxidative stress. *Methods Mol Biol*. 2007;371:179-189.
34. Lehle L, Tanner W. The specific site of tunicamycin inhibition in the formation of dolichol-bound *N*-acetylglucosamine derivatives. *FEBS Lett*. 1976;71:167-170.
35. Foufelle F, Fromenty B. Role of endoplasmic reticulum stress in drug-induced toxicity. *Pharmacol Res Perspect*. 2016;4:e00211.
36. Nakanishi K, Dohmae N, Morishima N. Endoplasmic reticulum stress increases myofiber formation in vitro. *FASEB J*. 2007;21:2994-3003.
37. Eo H, Valentine RJ. Imoxin inhibits tunicamycin-induced endoplasmic reticulum stress and restores insulin signaling in C2C12 myotubes. *Am J Physiol Cell Physiol*. 2021;321:C221-C229.

38. Thiel C, Lübke T, Matthijs G, von Figura K, Körner C. Targeted disruption of the mouse phosphomannomutase 2 gene causes early embryonic lethality. *Mol Cell Biol*. 2006;26:5615-5620.
39. Cornelison DDW. Context matters: in vivo and in vitro influences on muscle satellite cell activity. *J Cell Biochem*. 2008;105:663-669.
40. Jaeken J, Lefeber D, Matthijs G. Clinical utility gene card for: DPAGT1 defective congenital disorder of glycosylation. *Eur J Hum Genet*. 2015;23:1-3.
41. Ng BG, Underhill HR, Palm L, et al. DPAGT1 deficiency with encephalopathy (DPAGT1-CDG): clinical and genetic description of 11 new patients. *JIMD Rep*. 2018;44:85-92.
42. Witters P, Honzik T, Bauchart E, et al. Long-term follow-up in PMM2-CDG: are we ready to start treatment trials? *Genet Med*. 2019;21:1181-1188.
43. Muthusamy K, Perez-Ortiz JM, Ligezka AN, et al. Neurological manifestations in PMM2-congenital disorders of glycosylation (PMM2-CDG): insights into clinico-radiological characteristics, recommendations for follow-up and future directions. *Genet Med*. 2023;26:101027.
44. Footitt EJ, Karimova A, Burch M, et al. Cardiomyopathy in the congenital disorders of glycosylation (CDG): a case of late presentation and literature review. *J Inherit Metab Dis*. 2009;32:313-319.
45. Resende C, Carvalho C, Alegria A, et al. Congenital disorders of glycosylation with neonatal presentation. *BMJ Case Rep*. 2014;2014:bcr2013010037.
46. Aronica E, van Kempen AAMW, van der Heide M, et al. Congenital disorder of glycosylation type Ia: a clinicopathological report of a newborn infant with cerebellar pathology. *Acta Neuropathol*. 2005;109:433-442.
47. Wu R, Li D, Tang W, et al. Atrial septal defect in a patient with congenital disorder of glycosylation type 1a: a case report. *J Med Case Rep*. 2018;12:17.
48. Parkinson WM, Dookwah M, Dear ML, et al. Neurological roles for phosphomannomutase type 2 in a new *Drosophila* congenital disorder of glycosylation disease model. *Dis Model Mech*. 2016;9:513-527.
49. Di Patria L, Annibalini G, Morrone A, et al. Defective IGF-1 prohormone N-glycosylation and reduced IGF-1 receptor signaling activation in congenital disorders of glycosylation. *Cell Mol Life Sci*. 2022;79:150.
50. Miller BS, Khosravi MJ, Patterson MC, Conover CA. IGF system in children with congenital disorders of glycosylation. *Clin Endocrinol*. 2009;70:892-897.
51. Arabkhari M, Bunda S, Wang Y, Wang A, Pshezhetsky AV, Hinek A. Desialylation of insulin receptors and IGF-1 receptors by neuraminidase-1 controls the net proliferative response of L6 myoblasts to insulin. *Glycobiology*. 2010;20:603-616.
52. Singh R, Chaudhary P, Arya R. Role of IGF-1R in ameliorating apoptosis of GNE deficient cells. *Sci Rep*. 2018;8:7323.
53. Velloso CP. Regulation of muscle mass by growth hormone and IGF-I. *Br J Pharmacol*. 2008;154:557-568.

SUPPORTING INFORMATION

Additional supporting information can be found online in the Supporting Information section at the end of this article.

How to cite this article: Annibalini G, Di Patria L, Valli G, et al. Impaired myoblast differentiation and muscle IGF-1 receptor signaling pathway activation after N-glycosylation inhibition. *The FASEB Journal*. 2024;38:e23797. doi:10.1096/fj.202400213RR